Inorganic Chemistry

Article

pubs.acs.org/IC

Highly Valence-Diversified Binuclear Uranium Complexes of a Schiff-Base Polypyrrolic Macrocycle: Prediction of Unusual Structures, Electronic Properties, and Formation Reactions

Jun Yao,[†] Xiu-Jun Zheng,[†] Qing-Jiang Pan,*[,†] and Georg Schreckenbach*[,‡]

[†]Key Laboratory of Functional Inorganic Material Chemistry of Education Ministry, School of Chemistry and Materials Science, Heilongjiang University, Harbin 150080, China

[‡]Department of Chemistry, University of Manitoba, Winnipeg, Manitoba R3T 2N2, Canada

Supporting Information

ABSTRACT: On the basis of relativistic density functional theory calculations, homo- and heterovalent binuclear uranium complexes of a polypyrrolic macrocycle in a U−O−U bridging fashion have been investigated. These complexes show a variety of oxidation states for uranium ranging from III to VI, which have been confirmed by the calculated electron-spin density on each metal center. An equatorially 5-fold uranyl coordination mode is suitable for hexavalent uranium complexes, while silylation of the uranyl oxo is favored by pentavalent uranium. Uranyl oxo ligands are not required anymore for the coordination environment of tetra- and trivalent uranium because of their replacement by strong donors such as tetrahydrofuran and iodine. Optimization of binuclear U^{VI}−U^{III} complexes with various coordinating modes of U^{III}, donor numbers, and donor types reveals that 0.5−1.0 electron has been transferred from U^{III} to U^{VI}. Consequently, U^{V}−U^{IV} complexes are more favorable. Electronic structures and formation reactions of several representative uranium complexes were calculated. For example, a 5f-based σ(U−U) bonding orbital is found in the diuranium(IV) complex, rationalizing the fact that it shows the shortest U−U distance (3.82 Å) among the studied binuclear complexes.

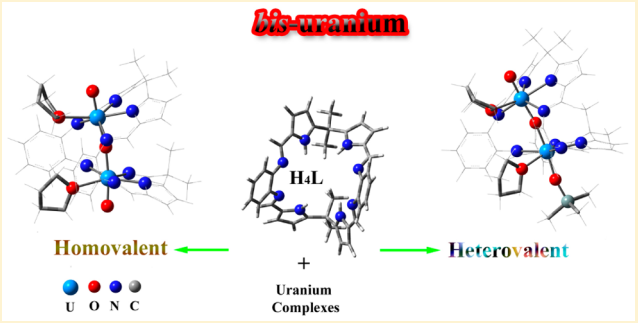

INTRODUCTION

Uranium has a diverse redox chemistry with four principal oxidation states of III−VI.[1−5] It is common to form approximately linear dioxo cations in the V and VI oxidation states, where the hexavalent uranyl (UO_2^{2+}) is especially well-known in most solutions and many solid media.[6−17] Because of its high mobility, the uranyl ion is the dominant uranium species in contaminated groundwater systems.[18−21] The redox chemistry of uranium has been widely utilized in its chemical separation.[22,23] Strategies to reduce the UO_2^{2+} mobility usually center on its reduction to insoluble uranium(IV) species. In contrast, the coordination chemistry of low-valent uranium(III) has flourished since starting materials such as $[UI_3(THF)_4]$,[24,25] $U[N(SiMe_3)_2]_3$,[25−27] and $[U(OTf)_3]$[28,29] were prepared by facile approaches. An increasing number of trivalent uranium complexes with various ligands and different coordination, solubility, and reactivity properties have been synthesized and characterized.[24−35]

Multiple oxidation states of uranium, however, may exist simultaneously in an aqueous environment, which makes its chemistry rather complex.[1,2] To shed light on this, binuclear uranium complexes, especially heterovalent bimetallic ones, are ideal candidates. More importantly, this will facilitate exploration of the structures of actinides, bonding properties and reactivity and further provide support for the safe processing and long-term immobilization of irradiated radionuclides. In this respect, it is a good choice to theoretically fabricate homo- and heterovalent diuranium complexes. Not only has relativistic quantum theory successfully predicted actinide structures and elucidated relevant properties,[4,5,36−44] but this approach avoids constraints imposed on experimental actinide chemistry by its chemical toxicity, radioactivity, and scarcity as well.

As a matter of fact, by the careful choice of ligands having suitable steric and electronic properties, it is possible to stabilize uranium within a wide range of oxidation states. Besides the use of multiple ligands,[6−12] expanded porphyrins, calixpyrroles, and related Schiff-base macrocycles have the ability to complex uranium ions.[45−60] For example, a flexible polypyrrolic macrocycle (H_4L in Chart 1), prepared independently by the Sessler[61] and Love[62] groups, is capable of accommodating two metal atoms such as actinide, lanthanide, and transition-metal atoms.[49−60] With the macrocycle ligand, Arnold, Love, and co-workers have successfully synthesized the diuranium(VI) complex $K_2[(UO_2)_2(\mu\text{-}O_2)(L)]$,[59] the diuranium(V) complex

Received: February 28, 2015
Published: May 8, 2015

DOI: 10.1021/acs.inorgchem.5b00483
Inorg. Chem. 2015, 54, 5438−5449

Chart 1. Flexible Polypyrrolic Macrocycle (H_4L)

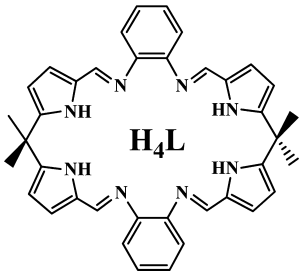

$[\{(Me_3Si)OU(\mu\text{-}O)\}_2(L)]$,[58] and diactinide(III) complexes $[(AnX)_2(L)]$ (An = U, X = I, BH_4; An = Np, X = I),[55] among others. Because the H_4L ligand is able to stabilize two uranium metal centers in the above oxidation states, we would question whether it is versatile enough to extend the complexation to two uranium(IV) atoms or even to binuclear complexes in a heterovalent mode (including oxidation states from III to VI). This has posed a challenge and also presented an opportunity for computational chemistry. Furthermore, binuclear complexes with mixed-valent uranium atoms are particularly attractive for both their fundamental interest in organometallic chemistry and their scarcity and underlying difficulty in experimental synthesis.

In this work, valence-diversified diuranium complexes of the Schiff-base polypyrrolic macrocycle (H_4L) have been examined using relativistic density functional theory (DFT). The calculated electron-spin density on each uranium center is used as evidence that these complexes have a variety of oxidation states from III to VI. It is found that tuning of the coordination environment of uranium is the key to obtaining various homo- and heterovalent diuranium complexes. The binuclear U^{VI}–U^{III} complex was calculated to be unfavorable; it readily switches to the analogous U^{V}–U^{IV} one. Electronic structures and reaction energies of several uranium complexes have been calculated in a tetrahydrofuran (THF) solution while considering the spin–orbit coupling (SOC) effects.

COMPUTATIONAL DETAILS

In this work, 50 diuranium complexes of the polypyrrolic macrocycle H_4L (Chart 1) with different oxidation states (III–VI) have been fully optimized using scalar relativistic DFT. Analytical frequency calculations have been performed to confirm the local minima nature of the stationary points on the potential energy surface. All of these optimized structures are presented in Figure S1 in the Supporting Information (SI). A structural feature of one oxygen bridging two uranium atoms, i.e., a U–O–U motif, was used to create the molecular skeleton, for a large number of binuclear uranium complexes with this mode have been experimentally reported.[59,63−70]

Structural and electron-spin analyses indicate that binuclear complexes with specific uranium oxidation states have a lot of commonality in their structures and properties. This will be shown by a detailed discussion of all possible geometries of U^{VI}–U^{III} complexes in the present work. Regarding U^{VI}–U^{m} (m = VI, V, and IV) and U^{n}–U^{n} (n = V, IV, and III) complexes, seven representative ones are focused on in the discussion (see Figure 1 for the U^{VI}–U^{m} complexes, Figure 2 for U^{VI}–U^{III}, and Figure 3 for U^{n}–U^{n}). In most cases, THF was used as the coordinating donor. Because of the considerable steric effects of THF, however, smaller-size water was adopted in the diuranium(V) complex, and iodine atoms were axially coordinated to the metal in the diuranium(III) complex (Figure 3).

It is well-known that a diuranium complex with multiple single electrons is capable of adopting many possible electronic states. In this work, we will present the structure with the highest electron-spin state. A binuclear U^{V}–U^{V} complex, for instance, has triplet and singlet electronic states. The triplet state is the subject herein. We have compared the two electronic states for seven diuranium(V) complexes (Figure S2 and Table S1 in the SI). It is shown that the triplet state is energetically lower than its corresponding singlet state, giving confidence in our approach.

The *Priroda* code (version 6)[71−75] was used to optimize the structures of the complexes in the gas phase without any symmetry constraints. We applied the generalized gradient approximation Perdew–Burke–Ernzerhof (GGA-PBE) functional[76] in these calculations, associated with all-electron (AE) correlation-consistent Gaussian basis sets of double-ζ-polarized quality for the large component and corresponding kinetically balanced basis sets for the small component.[72] The calculation on the U^{VI}–U^{V} complex $[(THF)(OU^{VI})(\mu\text{-}O)\{U^{V}O(SiMe_3)\}(THF)(L)]^{2+}$ (Figure 1), for instance, includes 122 atoms and 643 electrons; the basis sets were taken as U(34s33p24d18f6g)/(10s9p7d4f1g), Si(14s13p11d6f)/(9s7p5d2f), O(10s7p3d)/(3s2p1d), N(10s7p3d)/(3s2p1d), C-(10s7p3d)/(3s2p1d), and H(6s2p)/(2s1p), and thus 1389 orbital basis functions with 4076 auxiliary basis functions were used. A scalar relativistic four-component AE approach[74,77] was used to describe relativistic effects. The approach arises from the full Dirac equation but with spin–orbit projected out[78] and neglected. In addition to confirming that the optimized structures are local minima on the potential energy surface, analytical frequency results were also used to simulate the vibrational spectra via Lorentzian broadening (Figure S3 in the SI). Population-based (Mayer)[79] bond orders and atomic charges (Mulliken) were calculated. For comparison, other types of atomic charges including natural population analysis (NPA), Hirshfeld, and Voronoi were calculated using the *ADF* code[80−82] at various levels of theory.

To further understand the structural and reactivity properties of the actinide complexes, we have calculated the electronic properties of diuranium complexes using the *ADF 2010.02* code.[80−82] An

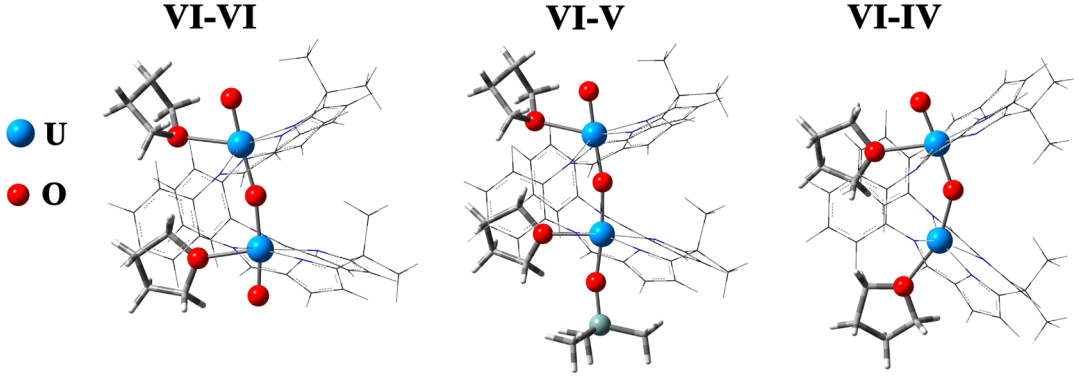

Figure 1. Optimized structures of binuclear U^{VI}–U^{m} (m = VI, V, and IV) complexes.

DOI: 10.1021/acs.inorgchem.5b00483
Inorg. Chem. 2015, 54, 5438−5449

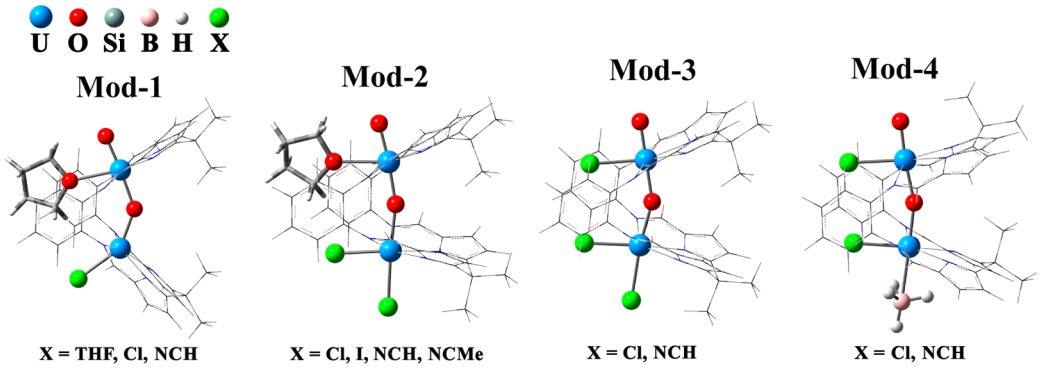

Figure 2. Optimized structures of binuclear U^{VI}–U^{III} complexes in various coordination models. See the text.

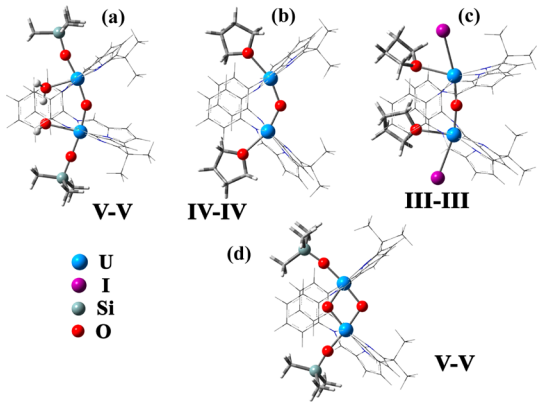

Figure 3. Optimized structures of homovalent U^m–U^m (m = V, IV, and III) complexes (a–c), compared with (d) a butterfly-like U^V–U^V complex (**B1**) that has been experimentally synthesized.[58]

integration parameter of 6.0 was applied. The PBE functional, the same as that for the optimizations, was applied. Because experimental uranyl complexes are isolated and characterized either in the solid state or in solution, we also considered environmental effects on their electronic structures. A continuum dielectric model, COSMO,[83,84] was employed with the dielectric constant (ε) of THF. Klamt radii were used for the uranium atom (1.70 Å)[85−89] and the main-group atoms (I = 1.90 Å, Si = 2.40 Å, O = 1.72 Å, N = 1.83 Å, C = 2.00 Å, and H = 1.30 Å).[90] The scalar relativistic ZORA method[91−94] and Slater-type TZP basis sets were used in these calculations. With the small-core ZORA-TZP basis sets, the core orbitals 1s–4f for U, 1s–4p for I, 1s–2p for Si, and 1s for C, N, and O were frozen.

Apart from the scalar relativity, the SOC effects[91,94] were included in further studies of formation reactions of $[(THF)(U^{VI}O_2)(H_2L)]$ (Mono-VI), $[(THF)_2(OU^{VI})_2(\mu\text{-}O)(L)]^{2+}$ (VI–VI), $[(THF)(OU^{VI}OU^{IV})(THF)(L)]^{2+}$ (VI–IV), and $[\{(THF)U^{IV}\}_2(\mu\text{-}O)(L)]^{2+}$ (IV–IV), where Mono-VI has been experimentally synthesized.[50] Additionally, comparisons were also made for the heterovalent VI–IV complex by varying the functional (GGA-PBE, hybrid B3LYP, and hybrid mPW1PW) and relativistic (scalar and SOC) effects and environmental media (solution and gas phase). The present results show that the pure GGA-PBE functional is sufficiently reliable for bimetallic systems, agreeing with previous studies.[95−99]

RESULTS AND DISCUSSION

Binuclear U^{VI}–U^m (m = VI, V, and IV) Complexes. *U^{VI}–U^{VI} Complexes.* The coordination chemistry of hexavalent uranyl has been well established by a large number of experimentally synthesized complexes; for some examples, see refs 6–17. The approximately linear *trans*-uranyl is equatorially coordinated by 4–6 ligands. According to this common coordination mode, we have created a similar environment for hexavalent uranium computationally. As shown in Figure 1, two uranium(VI) atoms feature a *trans*-uranyl skeleton, sharing

Table 1. Optimized Geometry Parameters and Bond Orders of Binuclear U^{VI}–U^m (m = VI, V, and IV) Complexes in the Gas Phase, Together with the Electron-Spin Density and Atomic Charge of Each Uranium Atom (Bond Lengths in Å and Angles in Degrees)

		calcd			exptl (U^{VI}–M)[a]		
		VI–VI	VI–V	VI–IV	Vac.	Mn	Co
U_1–O_{exo}		1.802 (2.47)[b]	1.799 (2.45)	1.800 (2.45)	1.766	1.768	1.771
U_1–O_{endo}		2.051 (1.15)	1.989 (1.43)	1.985 (1.43)	1.790	1.808	1.783
U_1–O_{eq}		2.480 (0.46)	2.585 (0.42)	2.551 (0.41)	2.442	2.458	2.474
U_2–O_{exo}/O_{ax}		1.801 (2.47)	2.000 (1.44)	2.420 (0.46)		2.216	2.117
U_2/M–O_{endo}		2.056 (1.16)	2.140 (0.90)	2.138 (0.89)		2.163	2.084
U_2–O_{eq}		2.561 (0.44)	2.485 (0.43)				
Si–O_{exo}			1.761 (0.89)				
U_1···U_2/M		4.088 (0.17)	4.113 (0.16)	3.944 (0.22)		3.804	3.726
O_{exo}–U_1–O_{endo}		172.4	176.7	176.9	177.6	177.4	177.8
O_{endo}–U_2–O_{exo}/O_{ax}		175.2	173.2	157.5		140.7	145.6
U_1–O_{endo}–U_2/M		169.0	169.7	146.1		146.5	148.8
spin (charge)	U_1^{VI}	0.000 (1.569)[c]	0.000 (1.521)	0.055 (1.610)			
	U_2^m	0.000 (1.660)	1.195 (1.934)	2.106 (1.717)			

[a]Experimental values of $[(THF)(UO_2)(H_2L)]$[50] and $[(THF)(OUOM)(THF)(L)]$ (M = Mn, Co)[51] complexes. [b]Calculated bond orders are listed in parentheses. [c]Calculated atomic charges are given in parentheses.

DOI: 10.1021/acs.inorgchem.5b00483
Inorg. Chem. 2015, 54, 5438–5449

an *endo*-oxo atom. Each metal center adopts a 5-fold coordination mode in its equatorial plane, of which four coordination sites are occupied by the N_4 donors of one compartment of the polypyrrolic ligand and the fifth is donated by an extra THF solvent.

Optimization (Table 1) of the binuclear uranium(VI) complex results in an U═O_{exo} bond length of 1.80 Å with a bond order of 2.47, which is comparable to those in experimentally obtained[6−17] and theoretically studied[39,88,89,100,101] uranyl complexes. The calculated U═O_{endo} distance is about 0.25 Å longer, associated with a much smaller bond order of 1.15. The U−O_{eq} distances range from 2.48 to 2.56 Å, being of dative-bond nature with bond orders of 0.45 on average. These two O_{eq} atoms of the two THF ligands significantly deviate from the U−N_4 plane by 1.02 and 1.91 Å. An optimized U···U separation of 4.09 Å was obtained for the binuclear uranium(VI) complex. There is no implication of any metal−metal bonding interaction because the U−O_{endo}−U angle was calculated to be approximately linear (169°) and the small U···U bond order (0.17) was apparently contributed by interaction of the electron density around the *endo*-oxo atom with the positively charged uranium atoms.

In addition, it is found that changes of the equatorial ligands from 2THF to neutral $2OH_2$ and $2OMe_2$, negative $2OH^-$, and mixed OH_2/OH^- (Figure S1 in the SI) do not cause large changes in the geometries of their corresponding complexes. Thus, only the complexes coordinated by THF will be discussed in the following text.

U^{VI}−U^{V} Complexes. Building on previous experimental and theoretical studies, one can readily assume the coordination environment of pentavalent uranium to be the same as that of the hexavalent one, i.e., a linear *trans*-UO_2^+ feature equatorially ligated by five donors. So, we shall investigate binuclear U^{VI}−U^{V} complexes directly using the geometry of the corresponding optimized U^{VI}−U^{VI} complex. Unexpectedly, some electron transfer is found from U^{V} to U^{VI}. For example, the symmetrical $[(OU^{VI})(\mu\text{-}O)(U^{V}O)(L)]^+$ (Mod-1 in Figure S1 in the SI), where the two uranium atoms have equivalent chemical coordination environments, yields 0.46 and 0.77 electrons localized on the two metal centers. Apparently, a single electron that is supposed to be residing in U^{V} of the expected binuclear U^{VI}−U^{V} complex has been roughly averaged to be distributed over the two uranium atoms.

Very recently, Parthey and Kaupp[102] have suggested that hybrid functionals with about 30−45% exact-exchange admixture would provide a reasonable compromise for heterovalent transition-metal complexes, when augmented by an appropriate treatment of (solvent or solid-state) environmental effects. Accordingly, the mPW1PW (containing 42.8% HF exchanges), B3LYP (20%), and PBE (0%) functionals implemented in the *ADF* code were used to calculate $[(OU^{VI})(\mu\text{-}O)(U^{V}O)(L)]^+$, while employing the COSMO model for environmental simulation. The electron-spin density of U^{VI}/U^{V} was calculated to be 0.00/1.13, 0.00/1.08, and 0.45/0.79, respectively. We conclude that the hybrid functionals successfully eliminate possible "delocalization errors" for the symmetric heterovalent systems.

Excellent experimental work on pentavalent uranium[52,103,104] has further enlightened us. Specifically, silylation of a uranyl *exo*-oxo atom of mononuclear $[(THF)(U^{VI}O_2)(H_2L)]$ allows easy reduction from U^{VI} to U^{V}.[52−54] According to this type of complex, we have designed a binuclear U^{VI}−U^{V} complex, $[(THF)(OU^{VI})(\mu\text{-}O)\{U^{V}O(SiMe_3)\}(THF)(L)]^{2+}$ (Figure 1), where one silyl group is added onto the *exo*-oxo atom of one uranyl. In this manner, slightly different chemical environments have been applied for the uranium(VI) and -(V) atoms, which completely eliminates the case of equivalent metal atoms. As a result, a truly heterovalent U^{VI}−U^{V} complex has been obtained even at the GGA-PBE level because a 0.00 electron-spin density has been found at the uranium(VI) atom while 1.20 electron is situated around U^{V} (Table 1).

The optimized geometry of this complex yields a long U^{V}═O_{exo} bond length at 2.00 Å. This is close to the experimental values of 1.99 Å in $[(THF)\{(Me_3Si)OU^{V}OM_2I_2\}(L)]$ (M = Fe, Zn),[52] 2.00 Å in $[U^{V}(OSiMe_3)_2I_2(^{Ar}acnac)]$ [^{Ar}acnac = ArNC(Ph)CHC(Ph)O; Ar = 3,5-^{t}Bu$_2$C$_6$H$_3$],[104] and 2.01 Å in $[\{(Me_3Si)OU(\mu\text{-}O)\}_2(L)]$.[58] Our calculated U^{V}═O_{exo}(−Si) distance is a little longer than the experimental U^{V}═O_{exo}(−M) (M = Li^+, K^+, Tl^{3+}, U^{5+})[54,105−110] distances of 1.85−1.92 Å because the O_{exo}−M interaction (so-called cation−cation interaction) is obviously weaker than the O_{exo}−Si covalent bond. In addition, elongation (by about 0.16−0.18 Å) is found in comparison with experimentally known pentavalent uranyl complexes such as $[(U^{V}O_2)(OPPh_3)_4](OTf)$,[9] $[(U^{V}O_2)(py)_5]$-[I]·py,[110] and $[(U^{V}O_2)(OTf)(py)_4]$[110] that possess a bare uranyl *exo*-oxo atom (OTf is triflate).

In this binuclear U^{VI}−U^{V} complex, the bond order of the U^{V}═O_{exo} bond was calculated to be 1.44, indicative of a bond that is weaker than a normal double bond. The O_{endo}−U^{V}−O_{exo} and U^{V}−O_{exo}−Si angles are 173° and 166°, agreeing with the experimental values[52,58,104] of 172° and 163° (mean values), respectively. The U^{VI}═O_{exo} bond length in the same molecule was calculated at 1.80 Å with a bond order of 2.45, corresponding to the usual partial triple bond. Again, a long U···U separation (4.11 Å) is found. Our designed U^{VI}−U^{V} complex $[(THF)(OU^{VI})(\mu\text{-}O)\{U^{V}O(SiMe_3)\}(THF)(L)]^{2+}$ is comparable to the experimentally synthesized $[(U^{VI}O_2)$-$(BIPMH)(\mu\text{-}Cl)U^{V}O(\mu\text{-}O)(BIPMH)]$ [BIPMH = HC-$(PPh_2NSiMe_3)_2$].[70]

U^{VI}−U^{IV} Complexes. By mimicking the experimentally known bimetallic complexes $[(THF)(OUOM)(THF)(L)]$ (M = Mn, Fe, Co),[51] we have successfully optimized a heterovalent U^{VI}−U^{IV} complex, as shown in Figure 1. The heterovalent nature of the diuranium complex is confirmed by the calculated spin density. A negligible 0.06 electron spin is distributed on the uranium(VI) atom, and a 2.11 spin is localized on the uranium(IV) atom. In this complex, the tetravalent uranium does not possess the linear uranyl molecular skeleton. The U^{IV}−O_{endo} and U^{IV}−O(THF) bond lengths were calculated at 2.14 and 2.42 Å, respectively. This structural feature actually resembles the uranium(IV) complexes found in the experimental synthesis.[111−114] It is worth pointing out that the hexavalent uranyl is rigid enough to be retained throughout in the above-discussed U^{VI}−U^{m} (m = VI, V, and IV) complexes (Table 1).

Atomic Charge and Electron Spin. The atomic charge and electron-spin density have been calculated for the binuclear U^{VI}−U^{m} (m = VI, V, and IV) complexes (Table 1 and more detailed information in Table S2 in the SI). The atomic charges of U^{VI} change slightly along the series, i.e., +1.57 and +1.66 in the diuranium(VI) complex, +1.52 in the U^{VI}−U^{V} complex, and +1.61 in the U^{VI}−U^{IV} complex, although they are far lower than the formal oxidation state of uranium (6+). It is surprising that more positive charges were calculated for the second uranium atom, +1.93 for U^{V} in the U^{VI}−U^{V} complex and +1.72 for U^{IV} in the U^{VI}−U^{IV} complex. This absolutely destroys any possible

DOI: 10.1021/acs.inorgchem.5b00483
Inorg. Chem. 2015, 54, 5438−5449

simple correlation that the atomic charge is increasing with increased oxidation state. Further NPA of the U^{VI}–U^{IV} complex at the *ADF*: PBE/Gas level shows similar charges of 1.50 for U^{VI} and 1.99 for U^{IV} (see Table S3 in the SI). At the other levels of theory (*ADF*: PBE/Sol, B3LYP/Sol, mPW1PW/Sol, and mPW1PW/Gas), the calculated Mulliken charges of the uranium atoms, for example, remain much lower than their formal oxidation states. Very similar cases are found for other binuclear uranium complexes (U^m–U^m, where m = VI–III) at the *ADF*: PBE/Sol level (Table S4 in the SI). In other words, it is impossible to make use of the calculated atomic charges to identify the oxidation state of uranium in these diuranium complexes.

On the other hand, the calculated electron-spin density is a good indicator to identify the oxidation state of the uranium atom. The present studies indicate that the GGA-PBE functional can precisely calculate the electron spin of the homovalent diuranium complexes and the heterovalent systems with the different coordination environments for two uranium centers (i.e., unsymmetrical structural systems). For example, the uranium centers with oxidation states of VI, V, and IV in the above complexes (Table 1) display electron-spin densities of ∼0.00, 1.20, and 2.11, respectively, corresponding to zero, one, and two 5f single electrons; the unsymmetrical homovalent U^{VI}–U^{IV} complex (Table S3 in the SI) shows 0.17/2.09, 0.01/2.11, and 0.01/2.13 for U^{VI}/U^{IV} at the *ADF*: PBE/Sol, B3LYP/Sol, and mPW1PW/Sol levels, respectively, close to the value of 0.06/2.11 at the *Priroda*: PBE/Gas level. Regarding the symmetrical heterovalent systems (as indicated above for $[(OU^{VI})(\mu\text{-}O)(U^{V}O)(L)]^{+}$), however, the hybrid functionals are capable of eliminating possible "delocalization errors", in contrast to the roughly averaged results of the GGA-PBE functional. Because the present study focuses on the unsymmetrical heterovalent diuranium complexes, the GGA-PBE functional is sufficiently accurate for their calculations.

Tuning the Structures of U^{VI}–U^{III} Complexes. Optimizing the heterovalent U^{VI}–U^{III} complex is not an easy task. The U^{6+} ion is formed by losing all of the six 5f valence electrons. Therefore, it is in an electron-deficient state. On the other hand, the U^{3+} ion retains its three 5f single electrons and is electron-rich accordingly. Therefore, electron transfer from U^{III} to U^{VI} is most likely to occur, especially given that there is an oxo ligand to bridge them. In accordance with this picture, optimizations at the GGA-PBE level demonstrate that the heterovalent U^{V}–U^{IV} complexes are favored over their U^{VI}–U^{III} counterparts. Further hybrid functional calculations also support this conclusion, as seen in Table S5 in the SI.

We have designed four different coordination modes to model the binuclear U^{VI}–U^{III} complex (Figure 2). In each case, the coordination environment of the hexavalent uranyl ion is adopted at the uranium(VI) atom end, while that of U^{III} has been varied greatly. Models 1 and 2, for instance, include variations of the number (one and two) of ligands, donating ability (THF, Cl, and I), and electronic properties (σ of Cl and I, as well as π of NCH and NCMe). As shown in Table 2, the obtained structure is best described as a U^{V}–U^{IV} complex in each case because 0.53–1.10 electron is localized on the uranium(VI) atom that is supposed to be zero and 2.12–2.40 electron is distributed over the expected uranium(III) atom. The optimized geometry parameters (Table 3) also support a pentavalent uranium structure. The $U_1{=}O_{exo}$ bond lengths were calculated to be within 1.81–1.83 Å, close to the experimental $U^{V}{=}O$ values[9,53,54,105−110] and longer than the

Table 2. Calculated Electron-Spin Densities Localized around Each Uranium Atom for Heterovalent U^{VI}–U^{III} Complexes, Which Are Effectively U^{V}–U^{IV} Ones

	$X_{eq/ax}$	$U_1^{VI\leftrightarrow V}$	$U_2^{III\leftrightarrow IV}$
Mod-1	THF	0.889	2.334
	Cl	1.057	2.167
	HCN	0.700	2.371
Mod-2	Cl	1.100	2.123
	I	1.096	2.171
	HCN	0.532	2.397
	MeCN	0.688	2.360
Mod-3	Cl	0.975	2.178
	HCN	0.548	2.376
Mod-4	Cl	1.120	2.055
	HCN	1.014	2.082

1.80 Å $U^{VI}{=}O_{exo}$ distances calculated for the binuclear U^{VI}–U^m (m = VI, V, and IV) complexes. It is also found that ligands NCH and NCMe with π-donating ability are capable of reducing, to some extent, electron transfer from U^{III} to U^{VI} but cannot completely stop this electron transfer.

Further attempts were also made by changing the fifth ligand of the hexavalent uranyl simultaneously (Mod-3 and Mod-4) and even introducing a BH_4^- group to stabilize the trivalent uranium (Mod-4). Optimizations while replacing BH_4^- with BF_4^- and BF_3 were not successful. The expected U^{VI}–U^{III} structure was not obtained for these complexes either, as seen in Tables 2 and 3; the U^{V}–U^{IV} structure is still preferred. So what is the reason? First of all, there exists a spontaneous driving force, i.e., a thermodynamic motivation that an electron flows from the electron-rich U^{III} to the electron-poor U^{VI}. One can note that complexes coordinated by halide atoms (some of the complexes in Mod-1 to Mod-3) and by a BH_4^- group (all complexes in Mod-4) are completely changed into their U^{V}–U^{IV} counterparts (Table 2) because they have ∼1.0 and ∼2.0 electrons on the respective metal centers. These complexes have essentially localized electrons on the uranium(V) and -(IV) centers and thus feature small U–U bond orders between 0.16 and 0.27. However, other complexes show an obvious resonance feature between U^{VI}–U^{V} and U^{III}–U^{IV}, displaying 0.53–0.89 and 2.33–2.38 electron-spin density, respectively. This dynamic electron exchange causes charge-transfer interaction between the two uranium centers. Consequently, relatively large U–U bond orders of 0.48–0.60 were calculated for these complexes, albeit with long distances of 3.82–4.08 Å. Second, the oxo-bridging structure (U–O–U) would facilitate this charge-transfer process from U^{III} to U^{VI} to some degree. Last but not the least, the *trans*-UO_2 structure is also suitable for the uranium(V) atom. Consequently, heterovalent U^{V}–U^{IV} complexes were obtained in these calculations instead of U^{VI}–U^{III} complexes.

Finally, we can propose an optimal U^{V}–U^{IV} structure (as shown in Figure S4 in the SI) based on the results of the present study. In this structure, one silyl is added onto the uranyl *exo*-oxo atom to fabricate an optimal environment for the pentavalent uranium. In addition, the uranyl *endo*-oxo atom directly coordinates to the tetravalent uranium that is axially saturated by a THF ligand. The optimized structural parameters of this complex are shown in Table 3.

Homovalent U^m–U^m (m = V, IV, and III) Complexes. The above results regarding uranium in various oxidation states can readily be extended to the study of homovalent U^m–U^m (m

DOI: 10.1021/acs.inorgchem.5b00483
Inorg. Chem. 2015, 54, 5438–5449

Table 3. Optimized Geometry Parameters and Corresponding Bond Orders (in Italic Font in the Following Row) of Binuclear U^{VI}–U^{III} Complexes in the Gas Phase (Bond Lengths in Å and Angles in Degrees)

	$X_{eq/ax}$	U_1–O_{exo}	U_1–O_{endo}	U_1–X_{eq}	U_2–O_{endo}	U_2–$X_{eq/ax}$	U_2–H	U_1···U_2	α_1[a]	α_2[a]	α_3[a]
Mod-1	THF	1.816	2.063	2.611	2.074	−/2.491		3.820	176.4	161.5	134.9
		2.46	*1.21*	*0.35*	*1.13*	*−/0.40*		*0.48*			
	Cl	1.823	2.054	2.592	2.090	−/2.599		3.896	176.2	146.7	140.2
		2.44	*1.24*	*0.35*	*1.10*	*−/1.22*		*0.27*			
	HCN	1.811	2.024	2.575	2.117	−/2.513		3.890	174.9	148.3	139.9
		2.45	*1.31*	*0.37*	*1.01*	*−/0.45*		*0.56*			
Mod-2	Cl	1.831	1.987	2.594	2.183	2.645/2.622		4.130	175.0	176.2	164.2
		2.43	*1.49*	*0.32*	*0.85*	*1.10/1.11*		*0.16*			
	I	1.830	2.003	2.565	2.148	3.121/3.069		4.132	173.6	173.7	168.9
		2.43	*1.44*	*0.33*	*0.90*	*1.00/1.08*		*0.17*			
	HCN	1.808	1.964	2.560	2.178	2.501/2.573		4.082	175.3	173.5	160.5
		2.44	*1.52*	*0.37*	*0.83*	*0.43/0.38*		*0.57*			
	MeCN	1.812	1.987	2.575	2.144	2.531/2.598		4.083	174.5	169.9	162.3
		2.45	*1.44*	*0.35*	*0.89*	*0.44/0.37*		*0.56*			
Mod-3	Cl	1.838	2.015	2.660	2.163	2.629/2.668		4.090	179.6	173.3	156.4
		2.43	*1.41*	*1.10*	*0.91*	*1.15/1.04*		*0.26*			
	HCN	1.812	1.964	2.656	2.190	2.519/2.580		3.952	170.9	178.4	144.0
		2.45	*1.53*	*0.28*	*0.80*	*0.46/0.37*		*0.60*			
Mod-4	Cl	1.837	2.060	2.662	2.108	2.618/2.628	2.442	4.116	175.2	178.6	161.9
		2.40	*1.32*	*1.11*	*1.01*	*1.21/0.36*	*0.16*	*0.17*			
	HCN	1.823	2.030	2.698	2.119	2.560/2.578	2.381	4.043	179.0	166.7	154.1
		2.43	*1.38*	*0.27*	*0.96*	*0.39/0.40*	*0.19*	*0.25*			
	X_{ax}	U_1–O_{exo}	U_1–O_{endo}	U_1–O_{eq}	U_2–O_{endo}	U_2–O_{ax}	Si–O_{exo}	U_1···U_2	α_1[a]	α_2[a]	α_3[a]
V–IV[b]	THF	2.005	2.054	2.560	2.078	2.432	1.756	3.919	178.9	160.6	143.0
		1.42	*1.24*	*0.39*	*1.12*	*0.45*	*0.91*	*0.20*			

[a] α_1, α_2, and α_3 denote angles of O_{exo}–U_1–O_{endo}, O_{endo}–U_2–X_{ax}, and U_1–O_{endo}–U_2, respectively. [b] The optimized structure of the binuclear U^V–U^{IV} complex is shown in Figure S4 in the SI. This complex has 1.189 and 2.102 electron-spin densities on the uranium(V) and -(IV) atoms, respectively.

Table 4. Optimized Geometry Parameters and Bond Orders (in Parentheses) for Binuclear U^m–U^m (m = V, IV, and III) Complexes in the Gas Phase, Together with Electron-Spin Density of Each Uranium Atom (Bond Lengths in Å and Angles in Degrees)

	calcd			calcd and exptl	
	V–V	IV–IV	III–III	V–V (**B1**)[a]	
U_1–O_{exo}/X_{ax}	1.996 (1.45)	2.440 (0.45)	3.238 (0.87)	2.048 (1.28)	2.034
U_1–O_{endo}	2.081 (1.14)	2.075 (1.17)	2.080 (1.16)	2.109 (1.19)/2.085 (1.23)	2.098/2.099
U_1–O_{eq}	2.502 (0.47)		2.710 (0.26)		
Si_1–O_{exo}	1.758 (0.89)			1.703 (1.03)	1.666
U_2–O_{exo}/X_{ax}	1.999 (1.43)	2.440 (0.44)	3.386 (0.65)	2.051 (1.26)	2.034
U_2–O_{endo}	2.068 (1.23)	2.075 (1.18)	2.088 (1.19)	2.101 (1.21)/2.111 (1.16)	2.098/2.099
U_2–O_{eq}	2.714 (0.33)		2.825 (0.24)		
Si_2–O_{exo}	1.757 (0.90)			1.702 (1.04)	1.666
U_1···U_2	3.999 (0.16)	3.819 (0.34)	4.156 (0.25)	3.379 (0.33)	3.356
O_{exo}/X_{ax}–U_1–O_{endo}	171.2	158.5	164.6	173.8/100.7	173.4/101.1
O_{endo}–U_2–O_{exo}/X_{ax}	171.6	158.8	166.4	173.3/100.5	173.4/100.5
U_1–O_{endo}–U_2	149.1	134.0	171.3	107.2/106.8	106.6/106.3
spin	1.166	2.126	2.684	1.125	
	1.150	2.125	2.522	1.126	

[a] Experimental values of the butterfly-like complex $[\{(Me_3Si)OU(\mu\text{-}O)\}_2(L)]$ (labeled as **B1** in the text) come from ref 58.

= V, IV, and III) complexes. Diuranium(V) complexes $[(X)_2\{(Me_3Si)OU^V\}_2(\mu\text{-}O)(L)]$ (X_2 = $2OH_2$, $2OH^-$, $2Cl^-$, and OH_2O^{2-}) have been obtained (see Mod-2 in Figure S1 and Table S1 in the SI). Regarding the equatorial X, we have tried to optimize large THF-coordinated and relatively small OMe_2-coordinated complexes but did not get converged results. This is obviously caused by their large steric effects. However, as shown in Figure 3a, the obtained complex $[(H_2O)_2\{(Me_3Si)OU^V\}_2(\mu\text{-}O)(L)]$ resembles the experimentally known uranium(V) complexes $[\{(Me_3Si)OU^V(\mu\text{-}O)\}_2(L)]$,[58] $[(THF)\{(Me_3Si)OU^VOM\}(THF)(L)]$,[52] and $[U^V(OSiMe_3)_2I_2(^{Ar}acnac)]$.[104] Optimization results in an approximate C_s symmetry for this OH_2-coordinated complex. Its triplet state is found to be the ground state, being 15.9 kcal/mol lower in energy than its singlet state. Thus, the two spins are arranged in parallel. The calculated spin densities on the uranium(V) atoms are 1.17 and 1.15 electrons.

DOI: 10.1021/acs.inorgchem.5b00483
Inorg. Chem. 2015, 54, 5438−5449

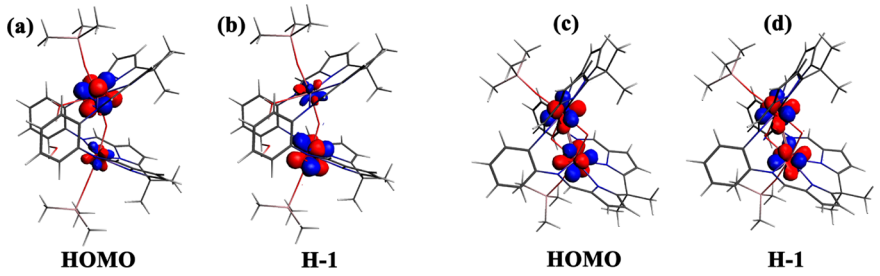

Figure 4. Diagrams of high-lying singly occupied U(f) orbitals for the binuclear U^{V}–U^{V} complex (a and b) compared with those of the butterfly-like diuranium(V) complex (c and d).

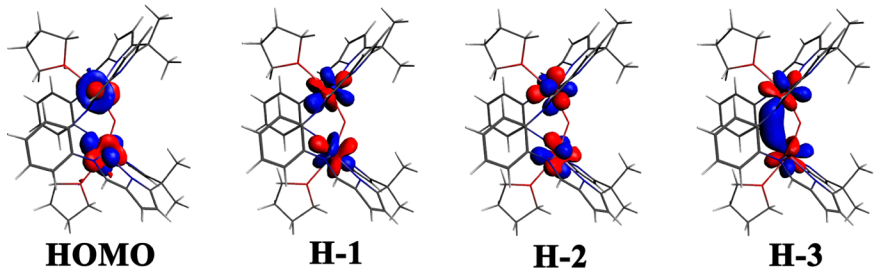

Figure 5. Diagrams of high-lying singly occupied U(f) orbitals for the binuclear U^{IV}–U^{IV} complex.

To further assess the present calculation, we also optimized the experimentally synthesized $[\{(Me_3Si)OU(\mu\text{-}O)\}_2(L)]$.[58] This butterfly-like complex is labeled as **B1**, as seen in Figures 3 and S2 in the SI. Excellent agreement between calculation and experiment has been achieved (Table 4). The differences in the $U{=}O_{exo/endo}$ bond lengths are less than 0.02 Å, and the angular deviations are no more than 1°. **B1** also possesses an electron-spin-parallel triplet ground state, which was calculated to be 14.2 kcal/mol lower in energy than its singlet state.

It is feasible to access a diuranium(IV) complex (Figure 3b) according to our above study. About 2.13 electrons have been calculated to be localized on each uranium atom, confirming that a binuclear tetravalent uranium complex can be obtained. It is worth noting that its U···U distance was calculated at 3.82 Å with a bond order of 0.34. This distance is the shortest one among the presently considered diuranium complexes (Tables 1, 3, and 4). Previous calculations of $U_2(OCHO)_4$[115] presented an outer minimum with a U–U distance of 3.42 Å that was assigned as a single σ bond. Comparatively, we therefore get a relatively weak U–U single bond in the diuranium(IV) complex, based on the U–U distance. Moreover, we can rule out the possibility that this U–U bonding interaction derives from contributions of charge transfer like the situation in the binuclear U^{VI}–U^{III} complexes because these two tetravalent uranium atoms are totally equivalent. Certainly, the unpaired electrons localized on the uranium(IV) centers and the small $U{-}O_{endo}{-}U$ angle of 134° also provide the necessary conditions for this U–U bonding. Further evidence will be given in the analysis of the electronic structures.

Again, the fabrication of diuranium(III) complexes finds that only 2.52–2.68 electrons (Table 4) are localized at each nominally trivalent uranium, even if the strong iodine donor is used. Inspection of the calculated results shows that about 0.75 electrons in total transfer to the polypyrrolic ligand. Further attempts using NCH and NCMe donors coordinating to uranium (Figure S1 in the SI) did not increase the electron-spin densities of uranium, corresponding to 2.53/2.50 and 2.52/2.61, respectively. Herein, we question whether the computational approach (GGA functional) might overestimate electron back-donation from the uranium(III) center to the ligand and, as a result, would not give accurate electron-spin values for the various trivalent uranium complexes. In order to further test this hypothesis, trivalent complexes $UI_3(THF)_4$, $UI_3(py)_4$, and $U[N(SiMe_3)_2]_3$ were calculated to display spin densities of 3.10, 2.84, and 3.09, respectively, using the same approach. The complex $UI_3(py)_4$ with the conjugated pyridine ligands shows a lower uranium spin, which further demonstrates significant electron transfer from metal to ligand. Therefore, we conclude that we can, indeed, obtain diuranium(III) complexes with the present approach; the back-donating effect from metal to ligand is responsible for the lower electron-spin density and not artifacts of the methodology.

Electronic Structures of Diuranium Complexes. On the basis of the above-optimized geometries, we have calculated the electronic structures of uranium complexes in a THF solution while employing the COSMO model. The binuclear U^{VI}–U^{VI} complex shows eight low-lying virtual orbitals of U(f) character, with the $\pi^*(U{=}O)$ ones lying above energetically. A total of 12 high-lying occupied orbitals are based on the polypyrrolic macrocycle ligand; in the bottom three (H-9 to H-11, where H-*n* stands for the orbital HOMO-*n*) of these orbitals, the aryl hinges are becoming dominant. Below them are the two orbitals contributed by the equatorial THF ligands. It is worth noting that all of the U=O bonding orbitals occur in a lower-energy area. The H-26 orbital, being 2.81 eV below the HOMO, is of primarily $\sigma(U{=}O)$ character, composed of 21% U(5f), 25% $O_{exo}(2p)$, and 4% $O_{endo}(2p)$ (Table S7 and Figure S5 in the SI).

With respect to the diuranium(V) complex, the two highest-energy orbitals are mainly occupied by the 5f single electrons (Figure 4). They are spin-parallel, showing a triplet ground state. These two α-spin orbitals are essentially degenerate and have similar character. No bonding interaction is found between the two uranium(V) atoms. Doubly occupied orbitals of silyl character are found in the low-energy area (H-14 to H-17). For comparison, we also present the 5f singly occupied

DOI: 10.1021/acs.inorgchem.5b00483
Inorg. Chem. 2015, 54, 5438–5449

orbitals of $[\{(Me_3Si)OU^{V}(\mu\text{-}O)\}_2(L)]$, which has been experimentally synthesized. This complex shows two equivalent 5f single-electron orbitals (Figure 4). The net $U^{V}-U^{V}$ bonding is still not found because of the essentially nonbonding 5f δ character[116] for the HOMO and H-1.

The diuranium(IV) complex has been optimized to show a short 3.82 Å U···U distance with a bond order of 0.34. According to the above structural analysis and comparison with a previous theoretical study,[115] a weak U−U single bond is presumed in the $U^{IV}-U^{IV}$ complex. Upon further inspection of the electronic structure, we find that the H-3 occupied by one 5f single electron is obviously of σ character, while the HOMO, H-1, and H-2 (5f ϕ and δ) are essentially nonbonding (Figure 5). Note that the H-3 does not include the oxo bridge. So, the effective formal bond order is 0.5, according to the electron occupation numbers. As seen in Figure 5, this σ bond is formed with an angle of ∼140°, different from a common head-to-head σ bond (∼180°), which results in a relatively weak U−U bonding and also rationalizes the calculated U−U bond order of 0.34. With the *ADF* code, the Mayer bond orders of U−U were calculated to be 0.75 and 0.72 in the gas phase and solution (Table S11 in the SI), respectively. A relatively weak $U^{IV}-U^{IV}$ bonding is confirmed, although the numerical value of the bond order is larger than the one from the *Priroda* code. The deviation is attributed to the difference of the basis sets used in the *ADF* and *Priroda* calculations. Our results agree with the previous conclusion of Bridgeman et al.[117] that the Mayer bond order shows significant basis-set dependence, especially for weak bonds. See also the detailed discussion in the SI.

Six 5f single electrons are included in the calculations of the diuranium(III) complex. The calculated electronic structure demonstrates that all of these electrons are α-spin and occupy six high-lying orbitals. The electron density is mainly localized on uranium in the HOMO, H-1, and H-2 (Figure S7 in the SI). However, pronounced electron transfer is found for the H-3, H-4, and H-5, as shown by ligand contributions of 15%, 22%, and 9%, respectively. This agrees with the conclusions of the structural and electron-spin density analyses above.

In Figure 6, we present characteristic orbitals of the heterovalent complex $[(THF)(OU^{VI}OU^{IV})(THF)(L)]^{2+}$ (VI−IV) calculated by various functionals (PBE, B3LYP, and mPW1PW). The PBE calculation yields singly occupied U(5f)-character HOMO and H-1 orbitals that are mainly contributed by the tetravalent uranium atom. Ligand-based doubly occupied character is found for the H-3 orbital. The density of states (DOS; Figures 7 and S8 in the SI) shows that the α-spin electrons contribute to the HOMO and H-1. The H-2 orbital is formed by one α electron and one β-spin electron that come from the polypyrrolic ligand. In contrast, the hybrid B3LYP and mPW1PW functionals give rise to different electronic structures, in addition to a wider HOMO−LUMO gap. However, from the point of view of the electronic arrangement, the PBE functional is sufficiently reliable to describe the heterovalent VI−IV complex. Additional calculations were also performed at the PBE/scalar ZORA/Gas and PBE/spin−orbit ZORA/Sol(THF) levels. A comparison reveals the same character and order of molecular orbitals at all three levels of theory (see Figure S9 in the SI). Therefore, the environmental media and extra SOC effect have only a slight effect on the electronic properties of the complex.

Reaction Energies of Uranium Complexes. The following reactions have been designed and calculated to

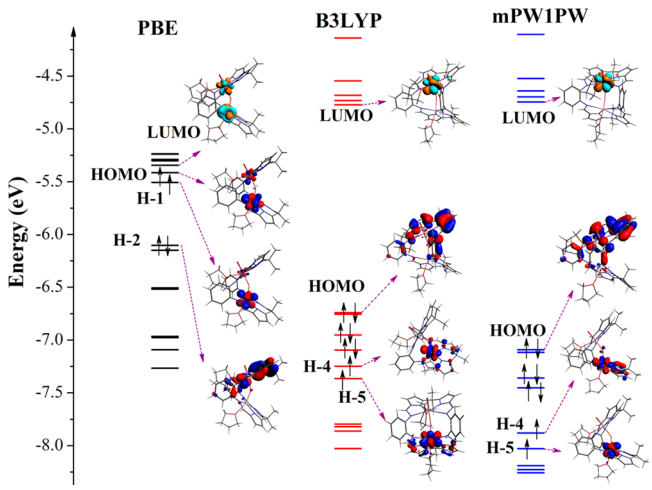

Figure 6. Characteristic U(f) and ligand-based orbitals of the heterovalent $U^{VI}-U^{IV}$ complex calculated by the PBE, B3LYP, and mPW1PW functionals, associated with the TZP basis sets, scalar ZORA relativistic effects, and COSMO solvation model. The α-spin orbital energy levels were used.

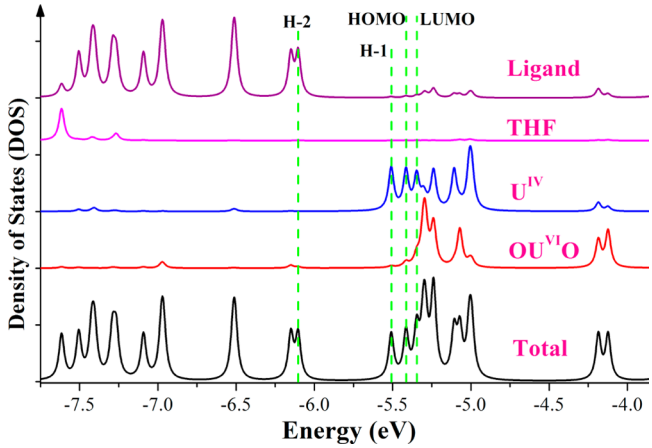

Figure 7. α-Spin DOS of the heterovalent $U^{VI}-U^{IV}$ complex calculated at the PBE/scalar ZORA/Sol(THF) level.

form mononuclear $[(THF)(U^{VI}O_2)(H_2L)]$ (Mono-VI), homovalent bimetallic $[(THF)_2(OU^{VI})_2(\mu\text{-}O)(L)]^{2+}$ (VI−VI) and $[\{(THF)U^{IV}\}_2(\mu\text{-}O)(L)]^{2+}$ (IV−IV), and heterovalent bimetallic $[(THF)(OU^{VI}OU^{IV})(THF)(L)]^{2+}$ (VI−IV). Hexavalent $[UO_2I_2(THF)_3]$ and tetravalent $[UI_4(THF)_3]$ were applied as uranium sources reacting with the H_4L polypyrrolic macrocyclic ligand in these reactions.

$$H_4L + [UO_2I_2(THF)_3] = [(THF)(U^{VI}O_2)(H_2L)]\ (\text{Mono-VI}) + 2HI + 2THF$$

$$H_4L + 2[UO_2I_2(THF)_3] = [(THF)_2(OU^{VI})_2(\mu\text{-}O)(L)]^{2+}\ (\text{VI} - \text{VI}) + 2HI + 2I^- + 4THF + H_2O$$

$$H_4L + [UO_2I_2(THF)_3] + [UI_4(THF)_3] = [(THF)(OU^{VI}OU^{IV})(THF)(L)]^{2+}\ (\text{VI} - \text{IV}) + 4HI + 2I^- + 4THF$$

DOI: 10.1021/acs.inorgchem.5b00483
Inorg. Chem. 2015, 54, 5438−5449

$$H_4L + 2[UI_4(THF)_3] + H_2O = [\{(THF)U^{IV}\}_2(\mu\text{-}O)(L)]^{2+}\ (IV-IV) + 6HI + 2I^- + 4THF$$

Solvation effects of THF were considered for all reactants and products at the PBE/scalar ZORA/COSMO level. Apart from the scalar relativistic effects, the SOC effects were calculated by introducing the spin−orbit-coupled ZORA. The results show that the SOC energy is as large as −424 kcal/mol for the Mono-VI complex and −855 kcal/mol (mean value) for the diuranium complexes. For the whole reaction, however, the free-energy contribution (ΔG_{so}) was calculated to be quite small, less than 2.5 kcal/mol (Table 5).

Table 5. Calculated Reaction Energies (kcal/mol) of Mono- and Binuclear Uranium Complexes in Oxidation States of VI and/or IV[a]

	Mono-VI[b]	VI−VI[b]	VI−IV[b]	IV−IV[b]
$\Delta_r E(\text{gas})$[c]	38.0	366.0	358.6	361.5
$\Delta_r E_0(\text{gas})$[c]	29.2	351.4	337.3	334.0
$\Delta_r H(\text{gas})$[c]	29.3	354.0	339.7	336.0
$\Delta_r G(\text{gas})$[c]	3.9	290.1	263.5	249.0
$\Delta_r G(\text{sol})$[d]	3.2	107.4	77.9	66.5
$\Delta_r G(\text{sol+so})$[d]	2.8	104.9	76.7	67.5
ΔG_{sol}[e]	−0.7	−182.7	−185.6	−182.5
ΔG_{so}[e]	−0.4	−2.5	−1.1	1.0

[a]See formation reactions in the text. [b]Calculated complexes are $[(THF)(U^{VI}O_2)(H_2L)]$ (Mono-VI), $[(THF)_2(OU^{VI})_2(\mu\text{-}O)(L)]^{2+}$ (VI−VI), $[(THF)(OU^{VI}OU^{IV})(THF)(L)]^{2+}$ (VI−IV), and $[\{(THF)\text{-}U^{IV}\}_2(\mu\text{-}O)(L)]^{2+}$ (IV−IV); see the text. [c]$\Delta_r E(\text{gas})$, $\Delta_r E_0(\text{gas})$, $\Delta_r H(\text{gas})$, and $\Delta_r G(\text{gas})$ denote the total energy, total energy including zero-point vibrational energy, enthalpy, and free energy of the reaction in the gas phase, respectively. [d]$\Delta_r G(\text{sol})$ stands for the reaction free energy in a THF solution, which includes scalar relativistic corrections and is calculated by $\Delta_r G(\text{sol}) = \Delta_r G(\text{gas}) + \Delta G_{sol}$. $\Delta_r G(\text{sol+so})$ is the reaction free energy, containing both the solvation effect and scalar and spin−orbit relativity, i.e., $\Delta_r G(\text{sol+so}) = \Delta_r G(\text{gas}) + \Delta G_{sol} + \Delta G_{so}$. [e]$\Delta G_{sol} = \sum \nu_B G_{sol}(B)$ and $\Delta G_{so} = \sum \nu_B G_{so}(B)$, where $G_{sol}(B)$ and $G_{so}(B)$ are the calculated solvation and SOC free energies of each molecule (B) in the formation reaction, respectively.

Different cases are found for the solvation free energy of reaction (ΔG_{sol}). Upon formation of Mono-VI, a ΔG_{sol} value of −0.7 kcal/mol was calculated, in contrast to −182 to −186 kcal/mol for the diuranium complexes. The difference in ΔG_{sol} can be qualitatively interpreted according to charges of the uranium complexes and the other reactants and products.[118] To first order, the solvation stabilization is proportional to the square of the charge and inversely proportional to the distance between the charge and polarizable medium. (This model would be exact for a point charge within the center of a spherical cavity.) So, ΔG_{sol} was calculated to be almost zero for the formation reaction of the *neutral* Mono-VI complex; because all of the reactants and products are neutral, a perfect cancellation is found in the whole reaction. However, large solvation energies ΔG_{sol} were calculated for other complexes. Careful inspection of their formation reactions finds that two parts contribute to these large values. First, the VI−VI, VI−IV, and IV−IV complexes, which have quite similar molecular sizes, carry two *positive* charges. Second, the I^- ion, which has one negative charge, provides a very large contribution because of its relatively small ionic radius.

In Table 5, we list reaction energies in the gas phase and THF solution. $\Delta_r G(\text{sol})$ includes solvation only, while $\Delta_r G(\text{sol+so})$ contains SOC as well. We plotted $\Delta_r G(\text{sol+so})$ in Figure 8. Thermodynamic calculations show that a small amount of

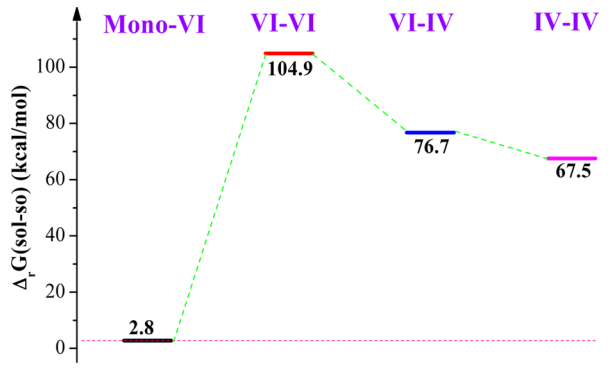

Figure 8. Free energies $\Delta_r G(\text{sol+so})$ of formation reactions of mono- and binuclear uranium complexes in oxidation states of VI and/or IV including both solvation and scalar/SOC relativistic effects.

energy (3.9 kal/mol) is required in the gas phase upon formation of the Mono-VI complex. Solvation and SOC have almost no effect on its formation reaction energy. The calculation agrees with the experimental result of the successful synthesis of the mononuclear complex Mono-VI.[50] A high endothermic reaction energy, 104.9 kcal/mol $\Delta_r G(\text{sol+so})$, was calculated for formation of the VI−VI complex because one stable uranyl bond has to be cleaved in this process. Comparatively, much lower $\Delta_r G(\text{sol+so})$ energies were calculated for the VI−IV (76.7 kcal/mol) and IV−IV (67.5 kcal/mol) complexes.

CONCLUSIONS

A series of homo- and heterovalent diuranium complexes have been examined using relativistic DFT for their structural, electronic, and reaction properties. The major conclusions can be summarized as follows:

Tuning of the coordination environment of uranium is a key way to obtain various homo- and heterovalent binuclear uranium complexes of different oxidation states. A uranyl coordination mode with five equatorial donors is suitable for a hexavalent uranium complex. The same model is applicable for pentavalent uranium; however, the coordination mode where the uranyl oxo is functionalized by silyl or an alkali-metal ion is strongly recommended instead. This mode has been shown to be more selective for the U^V oxidation state. The uranyl oxo structure is not required anymore for the coordination environment of tetra- and trivalent uranium. In these cases, it is replaced with strong donors such as THF and iodine.

The electron-spin density of uranium is a good indicator to identify the oxidation state of the uranium center, instead of the commonly used atomic charge, which has little predictive value. The GGA-PBE functional accurately predicts the electron spin of the metal center for the homovalent biuranium complexes and works well for the heterovalent systems with an unsymmetrical structural feature. Symmetrical heterovalent biuranium systems must be treated by hybrid functionals to eliminate possible "delocalization errors" because the GGA-PBE functional gives roughly averaged results for the spin

DOI: 10.1021/acs.inorgchem.5b00483
Inorg. Chem. 2015, 54, 5438−5449

density. Both GGA and hybrid functional calculations suggest that an unsymmetrical heterovalent $U^{V}-U^{IV}$ complex is much more favorable than its analogous $U^{VI}-U^{III}$.

Like the hybrid functional, pure PBE yields a reasonable description of the electronic properties of the heterovalent $U^{VI}-U^{IV}$ complex; moreover, variation of the relativistic levels (scalar and SOC) and environmental media (gas and solution) has only a slight effect. Regarding the homovalent $U^{m}-U^{m}$ (m = VI–III) complexes, high-lying occupied orbitals of macrocyclic ligand-based character are found for the diuranium(VI) and predominant U(5f)-character ones for other open-shell complexes. In most orbitals, U(5f) retains its character of the respective atomic orbital, showing no contribution to the U–U bonding. Interestingly, a weak σ(U–U) bond, derived from the overlap of two 5f orbitals in a nonlinear direction, has been assigned to the diuranium(IV) complex, which explains its short U–U distance of 3.82 Å and small but non-negligible bond order of 0.34. This calculated bond order does not arise from participation of the oxo bridge.

Thermodynamic calculations reveal that the SOC contribution to the reaction energy is quite small, while the role of solvation is significantly increased if the complex carries charges. A low reaction energy (<4 kcal/mol) was calculated for the Mono-VI complex that has been experimentally synthesized. However, it requires rather rigid conditions to synthesize the $U^{VI}-U^{VI}$ complex starting from hexavalent uranyl sources but relatively mild conditions to prepare the U^{IV}-containing complexes.

■ ASSOCIATED CONTENT

Supporting Information

Table of calculated electron spin densities and atomic charges of seven diuranium(V) complexes, together with their relative energies in different electronic states (Table S1), tables of detailed information on electron spin densities and atomic charges of diuranium complexes calculated with the *Priroda* and *ADF* codes (Tables S2–S6), tables of orbital compositions of homovalent diuranium complexes (Tables S7–S10), table of various $U^{IV}-U^{IV}$ bond orders calculated with the *ADF* code (Table S11), along with a discussion of U–U bonding, figure showing 50 polypyrrolic diuranium complexes with oxidation states of III–VI (Figure S1), structural drawings of seven diuranium(V) complexes (Figure S2), simulated IR vibrational spectra of $U^{VI}-U^{m}$ (m = VI–IV) and $U^{n}-U^{n}$ (n = V–III) complexes (Figure S3), optimized structure of the binuclear $U^{V}-U^{IV}$ complex (Figure S4), diagrams of orbital electron densities of binuclear $U^{m}-U^{m}$ (m = VI, V, and III) complexes (Figures S5–S7), and figure of the β-spin DOS of the homovalent $U^{VI}-U^{IV}$ complex (Figure S8), and diagrams of characteristic orbitals calculated at various relativistic levels and environmental media (Figure S9). The Supporting Information is available free of charge on the ACS Publications website at DOI: 10.1021/acs.inorgchem.5b00483.

■ AUTHOR INFORMATION

Corresponding Authors

*E-mail: panqjitc@163.com.
*E-mail: schrecke@cc.umanitoba.ca.

Notes

The authors declare no competing financial interest.

■ ACKNOWLEDGMENTS

This work is supported by the National Natural Science Foundation of China (21273063), the Program for New Century Excellent Talents in University (NCET-11-0958) and the Program for Innovative Research Team in University (IRT-1237). G.S. acknowledges financial support from the Natural Sciences and Engineering Research Council of Canada (NSERC, Discovery Grant). The authors are grateful to Dr. Dimitri Laikov for providing us with the *Priroda* code. G.S. and Q.-J.P. thank Polly Arnold and Jason Love at the University of Edinburgh for inspiring discussions that contributed to this work.

■ REFERENCES

(1) Hashke, J. M.; Stakebake, J. L. In *The chemistry of the actinide and transactinide elements*; Morss, L. R., Edelstein, N. M., Fuger, J., Eds.; Springer: New York , 2006; pp 3199–3272.
(2) Clark, D. L.; Hobart, D. E.; Neu, M. P. *Chem. Rev.* **1995**, *95*, 25–48.
(3) Kaltsoyannis, N.; Scott, P. *The f elements*; Oxford Science Publications: New York, 1999.
(4) Kaltsoyannis, N. *Chem. Soc. Rev.* **2003**, *32*, 9–16.
(5) Schreckenbach, G.; Shamov, G. A. *Acc. Chem. Res.* **2010**, *43*, 19–29.
(6) Berthet, J. C.; Lance, M.; Nierlich, M.; Ephritikhine, M. *Eur. J. Inorg. Chem.* **2000**, 1969–1973.
(7) Berthet, J. C.; Nierlich, M.; Ephritikhine, M. *Chem. Commun.* **2003**, 1660–1661.
(8) Berthet, J. C.; Nierlich, M.; Ephritikhine, M. *Chem. Commun.* **2004**, 870–871.
(9) Berthet, J. C.; Nierlich, M.; Ephritikhine, M. *Angew. Chem., Int. Ed.* **2003**, *42*, 1952–1954.
(10) Oldham, W. J.; Oldham, S. M.; Scott, B. L.; Abney, K. D.; Smith, W. H.; Costa, D. A. *Chem. Commun.* **2001**, 1348–1349.
(11) Vaughn, A. E.; Barnes, C. L.; Duval, P. B. *J. Chem. Crystallogr.* **2007**, *37*, 779–782.
(12) Wilkerson, M. P.; Burns, C. J.; Paine, R. T.; Scott, B. L. *Inorg. Chem.* **1999**, *38*, 4156–4158.
(13) Alcock, N. W.; Flanders, D. J.; Brown, D. *J. Chem. Soc., Dalton Trans.* **1985**, 1001–1007.
(14) Charpin, P.; Lance, M.; Nierlich, M.; Vigner, D.; Baudin, C. *Acta Crystallogr., Sect. C* **1987**, *43*, 1832–1833.
(15) Crawford, M.-J.; Ellern, A.; Karaghiosoff, K.; Mayer, P.; Noth, H.; Suter, M. *Inorg. Chem.* **2004**, *43*, 7120–7126.
(16) Crawford, M.-J.; Ellern, A.; Noth, H.; Suter, M. *J. Am. Chem. Soc.* **2003**, *125*, 11778–11779.
(17) Crawford, M.-J.; Mayer, P. *Inorg. Chem.* **2005**, *44*, 5547–5549.
(18) Choppin, G. R. *J. Radioanal. Nucl. Chem.* **2007**, *273*, 695–703.
(19) Thomas, S. H.; Padilla-Crespo, E.; Jardine, P. M.; Sanford, R. A.; Loffler, F. E. *Appl. Environ. Microbiol.* **2009**, *75*, 3679–3687.
(20) Mathews, T.; Beaugelin-Seiller, K.; Garnier-Laplace, J.; Gilbin, R.; Adam, C.; Della-Vedova, C. *Environ. Sci. Technol.* **2009**, *43*, 6684–6690.
(21) Rambo, B. M.; Sessler, J. L. *Chem.—Eur. J.* **2011**, *17*, 4946–4959.
(22) Jones, M. B.; Gaunt, A. J. *Chem. Rev.* **2013**, *113*, 1137–1198.
(23) Gorden, A. E. V.; Xu, J. D.; Raymond, K. N.; Durbin, P. *Chem. Rev.* **2003**, *103*, 4207–4282.
(24) Baker, R. J. *Coord. Chem. Rev.* **2012**, *256*, 2843–2871.
(25) Avens, L. R.; Bott, S. G.; Clark, D. L.; Sattelberger, A. P.; Watkin, J. G.; Zwick, B. D. *Inorg. Chem.* **1994**, *33*, 2248–2256.
(26) Andersen, R. A. *Inorg. Chem.* **1979**, *18*, 1507–1509.
(27) Monreal, M. J.; Thomson, R. K.; Cantat, T.; Travia, N. E.; Scott, B. L.; Kiplinger, J. L. *Organometallics* **2011**, *30*, 2031–2038.
(28) Berthet, J. C.; Lance, M.; Nierlich, M.; Ephritikhine, M. *Eur. J. Inorg. Chem.* **1999**, 2005–2007.

DOI: 10.1021/acs.inorgchem.5b00483
Inorg. Chem. 2015, 54, 5438–5449

(29) Natrajan, L.; Mazzanti, M.; Bezombes, J.-P.; Pécaut, J. *Inorg. Chem.* **2005**, *44*, 6115−6121.
(30) Arnold, P. L. *Chem. Commun.* **2011**, *47*, 9005−9010.
(31) Arnold, P. L.; Potter, N. A.; Carmichael, C. D.; Slawin, A. M. Z.; Roussel, P.; Love, J. B. *Chem. Commun.* **2010**, *46*, 1833−1835.
(32) Arnold, P. L.; Farnaby, J. H.; White, R. C.; Kaltsoyannis, N.; Gardiner, M. G.; Love, J. B. *Chem. Sci.* **2014**, *5*, 756−765.
(33) Patel, D.; Moro, F.; McMaster, J.; Lewis, W.; Blake, A. J.; Liddle, S. T. *Angew. Chem., Int. Ed.* **2011**, *50*, 10388−10392.
(34) Antunes, M. A.; Pereira, L. C. J.; Santos, I. C.; Mazzanti, M.; Marcalo, J.; Almeida, M. *Inorg. Chem.* **2011**, *50*, 9915−9917.
(35) Le Borgne, T.; Lance, M.; Nierlich, M.; Ephritikhine, M. *J. Organomet. Chem.* **2000**, *598*, 313−317.
(36) Wang, D.; van Gunsteren, W. F.; Chai, Z. *Chem. Soc. Rev.* **2012**, *41*, 5836−5865.
(37) Hayton, T. W.; Boncella, J. M.; Scott, B. L.; Palmer, P. D.; Batista, E. R.; Hay, P. J. *Science* **2005**, *310*, 1941−1943.
(38) Spencer, L. P.; Yang, P.; Minasian, S. G.; Jilek, R. E.; Batista, E. R.; Boland, K. S.; Boncella, J. M.; Conradson, S. D.; Clark, D. L.; Hayton, T. W.; Kozimor, S. A.; Martin, R. L.; MacInnes, M. M.; Olson, A. C.; Scott, B. L.; Shuh, D. K.; Wilkerson, M. P. *J. Am. Chem. Soc.* **2013**, *135*, 2279−2290.
(39) Pan, Q. J.; Schreckenbach, G.; Arnold, P. L.; Love, J. B. *Chem. Commun.* **2011**, *47*, 5720−5722.
(40) Gagliardi, L.; Roos, B. O. *Nature* **2005**, *433*, 848−851.
(41) La Macchia, G.; Brynda, M.; Gagliardi, L. *Angew. Chem., Int. Ed.* **2006**, *45*, 6210−6213.
(42) Gagliardi, L.; Roos, B. O. *Chem. Soc. Rev.* **2007**, *36*, 893−903.
(43) Li, J.; Bursten, B. E.; Liang, B. Y.; Andrews, L. *Science* **2002**, *295*, 2242−2245.
(44) Mills, D. P.; Moro, F.; McMaster, J.; van Slageren, J.; Lewis, W.; Blake, A. J.; Liddle, S. T. *Nat. Chem.* **2011**, *3*, 454−460.
(45) Sessler, J. L.; Mody, T. D.; Lynch, V. *Inorg. Chem.* **1992**, *31*, 529−531.
(46) Sessler, J. L.; Vivian, A. E.; Seidel, D.; Burrell, A. K.; Hoehner, M.; Mody, T. D.; Gebauer, A.; Weghorn, S. J.; Lynch, V. *Coord. Chem. Rev.* **2001**, *222*, 275−275.
(47) Sessler, J. L.; Seidel, D.; Vivian, A. E.; Lynch, V.; Scott, B. L.; Keogh, D. W. *Angew. Chem., Int. Ed.* **2001**, *40*, 591−594.
(48) Sessler, J. L.; Melfi, P. J.; Pantos, G. D. *Coord. Chem. Rev.* **2006**, *250*, 816−843.
(49) Love, J. B. *Chem. Commun.* **2009**, 3154−3165.
(50) Arnold, P. L.; Blake, A. J.; Wilson, C.; Love, J. B. *Inorg. Chem.* **2004**, *43*, 8206−8208.
(51) Arnold, P. L.; Patel, D.; Blake, A. J.; Wilson, C.; Love, J. B. *J. Am. Chem. Soc.* **2006**, *128*, 9610−9611.
(52) Arnold, P. L.; Patel, D.; Wilson, C.; Love, J. B. *Nature* **2008**, *451*, 315−318.
(53) Arnold, P. L.; Love, J. B.; Patel, D. *Coord. Chem. Rev.* **2009**, *253*, 1973−1978.
(54) Arnold, P. L.; Pecharman, A.-F.; Hollis, E.; Yahia, A.; Maron, L.; Parsons, S.; Love, J. B. *Nat. Chem.* **2010**, *2*, 1056−1061.
(55) Arnold, P. L.; Potter, N. A.; Magnani, N.; Apostolidis, C.; Griveau, J.-C.; Colineau, E.; Morgenstern, A.; Caciuffo, R.; Love, J. B. *Inorg. Chem.* **2010**, *49*, 5341−5343.
(56) Arnold, P. L.; Hollis, E.; White, F. J.; Magnani, N.; Caciuffo, R.; Love, J. B. *Angew. Chem., Int. Ed.* **2011**, *50*, 887−890.
(57) Arnold, P. L.; Pecharman, A.-F.; Love, J. B. *Angew. Chem., Int. Ed.* **2011**, *50*, 9456−9458.
(58) Arnold, P. L.; Jones, G. M.; Odoh, S. O.; Schreckenbach, G.; Magnani, N.; Love, J. B. *Nat. Chem.* **2012**, *4*, 221−227.
(59) Jones, G. M.; Arnold, P. L.; Love, J. B. *Angew. Chem., Int. Ed.* **2012**, *51*, 12584−12587.
(60) Arnold, P. L.; Hollis, E.; Nichol, G. S.; Love, J. B.; Griveau, J.-C.; Caciuffo, R.; Magnani, N.; Maron, L.; Castro, L.; Yahia, A.; Odoh, S. O.; Schreckenbach, G. *J. Am. Chem. Soc.* **2013**, *135*, 3841−3854.
(61) Sessler, J. L.; Cho, W. S.; Dudek, S. P.; Hicks, L.; Lynch, V. M.; Huggins, M. T. *J. Porphyrins Phthalocyanines* **2003**, *7*, 97−104.
(62) Givaja, G.; Blake, A. J.; Wilson, C.; Schroder, M.; Love, J. B. *Chem. Commun.* **2003**, 2508−2509.
(63) Bharara, M. S.; Heflin, K.; Tonks, S.; Strawbridge, K. L.; Gorden, A. E. V. *Dalton Trans.* **2008**, 2966−2973.
(64) Bharara, M. S.; Strawbridge, K.; Vilsek, J. Z.; Bray, T. H.; Gorden, A. E. V. *Inorg. Chem.* **2007**, *46*, 8309−8315.
(65) Tsushima, S. *Inorg. Chem.* **2012**, *51*, 1434−1439.
(66) Shvareva, T. Y.; Sullens, T. A.; Shehee, T. C.; Albrecht-Schmitt, T. E. *Inorg. Chem.* **2005**, *44*, 300−305.
(67) Wilkerson, M. P.; Burns, C. J.; Dewey, H. J.; Martin, J. M.; Morris, D. E.; Paine, R. T.; Scott, B. L. *Inorg. Chem.* **2000**, *39*, 5277−5285.
(68) Wilkerson, M. P.; Burns, C. J.; Morris, D. E.; Paine, R. T.; Scott, B. L. *Inorg. Chem.* **2002**, *41*, 3110−3120.
(69) Burns, C.; Sattelberger, A. *Inorg. Chem.* **1988**, *27*, 3692−3693.
(70) Mills, D. P.; Cooper, O. J.; Tuna, F.; McInnes, E. J. L.; Davies, E. S.; McMaster, J.; Moro, F.; Lewis, W.; Blake, A. J.; Liddle, S. T. *J. Am. Chem. Soc.* **2012**, *134*, 10047−10054.
(71) Laikov, D. N. *Chem. Phys. Lett.* **1997**, *281*, 151−156.
(72) Laikov, D. N. Ph.D. Thesis, Moscow State University, Moscow, Russia, 2000.
(73) Laikov, D. N. *Chem. Phys. Lett.* **2005**, *416*, 116−120.
(74) Laikov, D. N.; Ustynyuk, Y. A. *Russ. Chem. Bull.* **2005**, *54*, 820−826.
(75) Laikov, D. N. *J. Comput. Chem.* **2007**, *28*, 698−702.
(76) Perdew, J. P.; Burke, K.; Ernzerhof, M. *Phys. Rev. Lett.* **1996**, *77*, 3865−3868.
(77) Laikov, D. N. *An Implementation of the Scalar Relativistic Density Functional Theory for Molecular Calculatios with Gaussian Basis Sets*; DFT2000 Conference, Menton, France, 2000.
(78) Dyall, K. G. *J. Chem. Phys.* **1994**, *100*, 2118−2127.
(79) Mayer, I. *Simple theorems, proof and derivations in quantum chemistry*; Kluwer Academic /Plenum Publishers: New York, 2003.
(80) te Velde, G.; Bickelhaupt, F. M.; Baerends, E. J.; Fonseca Guerra, C.; Van Gisbergen, S. J. A.; Snijders, J. G.; Ziegler, T. *J. Comput. Chem.* **2001**, *22*, 931−967.
(81) Fonseca Guerra, C.; Snijders, J. G.; te Velde, G.; Baerends, E. J. *Theor. Chem. Acc.* **1998**, *99*, 391−403.
(82) Baerends, E. J.; Ziegler, T.; Autschbach, J. et al. *ADF 2010.02; SCM, Theoretical Chemistry*; Vrije Universiteit: Amsterdam, The Netherlands, 2010. See the full reference in the SI.
(83) Klamt, A.; Schuurmann, G. *J. Chem. Soc., Perkin Trans.* **1993**, 799−805.
(84) Pye, C. C.; Ziegler, T. *Theor. Chem. Acc.* **1999**, *101*, 396−408.
(85) Shamov, G. A.; Schreckenbach, G. *J. Phys. Chem. A* **2006**, *110*, 9486−9499.
(86) Pan, Q. J.; Odoh, S. O.; Schreckenbach, G.; Arnold, P. L.; Love, J. B. *Dalton Trans.* **2012**, *41*, 8878−8885.
(87) Pan, Q. J.; Schreckenbach, G.; Arnold, P. L.; Love, J. B. *Chem. Commun.* **2011**, *47*, 5720−5722.
(88) Pan, Q. J.; Shamov, G. A.; Schreckenbach, G. *Chem.—Eur. J.* **2010**, *16*, 2282−2290.
(89) Pan, Q. J.; Schreckenbach, G. *Inorg. Chem.* **2010**, *49*, 6509−6517.
(90) Klamt, A.; Jonas, V.; Burger, T.; Lohrenz, J. C. W. *J. Phys. Chem. A* **1998**, *102*, 5074−5085.
(91) van Lenthe, E.; Ehlers, A.; Baerends, E. J. *J. Chem. Phys.* **1999**, *110*, 8943−8953.
(92) van Lenthe, E.; Baerends, E. J.; Snijders, J. G. *J. Chem. Phys.* **1994**, *101*, 9783−9792.
(93) van Lenthe, E.; Baerends, E. J.; Snijders, J. G. *J. Chem. Phys.* **1993**, *99*, 4597−4610.
(94) van Lenthe, E.; Snijders, J.; Baerends, E. *J. Chem. Phys.* **1996**, *105*, 6505−6516.
(95) Infante, I.; Gagliardi, L.; Scuseria, G. E. *J. Am. Chem. Soc.* **2008**, *130*, 7459−7465.
(96) Wu, X.; Lu, X. *J. Am. Chem. Soc.* **2007**, *129*, 2171−2177.
(97) Gutsev, G. L.; Bauschlicher, C. W. *J. Phys. Chem. A* **2003**, *107*, 4755−4767.

DOI: 10.1021/acs.inorgchem.5b00483
Inorg. Chem. 2015, 54, 5438−5449

(98) Yanagisawa, S.; Tsuneda, T.; Hirao, K. *J. Chem. Phys.* **2000**, *112*, 545−553.
(99) Barden, C. J.; Rienstra-Kiracofe, J. C.; Schaefer, H. F., III. *J. Chem. Phys.* **2000**, *113*, 690−700.
(100) Shamov, G. A. *J. Am. Chem. Soc.* **2011**, *133*, 4316−4329.
(101) Ingram, K. I. M.; Häller, L. J. L.; Kaltsoyannis, N. *Dalton Trans.* **2006**, 2403−2414.
(102) Parthey, M.; Kaupp, M. *Chem. Soc. Rev.* **2014**, *43*, 5067−5088.
(103) Fortier, S.; Hayton, T. W. *Coord. Chem. Rev.* **2010**, *254*, 197−214.
(104) Brown, J. L.; Wu, G.; Hayton, T. W. *J. Am. Chem. Soc.* **2010**, *132*, 7248−7249.
(105) Burdet, F.; Pecaut, J.; Mazzanti, M. *J. Am. Chem. Soc.* **2006**, *128*, 16512−16513.
(106) Nocton, G.; Horeglad, P.; Pecaut, J.; Mazzanti, M. *J. Am. Chem. Soc.* **2008**, *130*, 16633−16645.
(107) Natrajan, L.; Burdet, F.; Pecaut, J.; Mazzanti, M. *J. Am. Chem. Soc.* **2006**, *128*, 7152−7153.
(108) Nocton, G.; Horeglad, P.; Vetere, V.; Pécaut, J.; Dubois, L.; Maldivi, P.; Edelstein, N. M.; Mazzanti, M. *J. Am. Chem. Soc.* **2009**, *132*, 495−508.
(109) Sullens, T. A.; Jensen, R. A.; Shvareva, T. Y.; Albrecht-Schmitt, T. E. *J. Am. Chem. Soc.* **2004**, *126*, 2676−2677.
(110) Berthet, J. C.; Siffredi, G.; Thuéry, P.; Ephritikhine, M. *Dalton Trans.* **2009**, 3478−3494.
(111) Schnaars, D. D.; Wu, G.; Hayton, T. W. *Dalton Trans.* **2008**, 6121−6126.
(112) Enriquez, A. E.; Scott, B. L.; Neu, M. P. *Inorg. Chem.* **2005**, *44*, 7403−7413.
(113) Berthet, J.-C.; Thuery, P.; Ephritikhine, M. *Inorg. Chem.* **2005**, *44*, 1142−1146.
(114) Berthet, J.-C.; Siffredi, G.; Thuery, P.; Ephritikhine, M. *Eur. J. Inorg. Chem.* **2007**, 4017−4020.
(115) Roos, B. O.; Gagliardi, L. *Inorg. Chem.* **2006**, *45*, 803−807.
(116) Gagliardi, L.; Pyykko, P.; Roos, B. O. *Phys. Chem. Chem. Phys.* **2005**, *7*, 2415−2417.
(117) Bridgeman, A. J.; Cavigliasso, G.; Ireland, L. R.; Rothery, J. *J. Chem. Soc., Dalton Trans.* **2001**, 2095−2108.
(118) Shamov, G. A.; Schreckenbach, G.; Martin, R. L.; Hay, P. J. *Inorg. Chem.* **2008**, *47*, 1465−1475.

DOI: 10.1021/acs.inorgchem.5b00483
Inorg. Chem. 2015, 54, 5438−5449